The Astrophysical Journal, 989:80 (10pp), 2025 August 10 https://doi.org/10.3847/1538-4357/ade3d7

Diversity of Cold Worlds: A Near-complete Spectral Energy Distribution for 2MASS J04151954−0935066 Using JWST

Sherelyn Alejandro Merchan[1,2], Jacqueline K. Faherty[1], Genaro Suárez[1], Kelle L. Cruz[1,2,3], Adam J. Burgasser[4], Jonathan Gagné[5,6], Callie E. Hood[7], Eileen C. Gonzales[8], Daniella C. Bardalez Gagliuffi[1,9], Jolie L'Heureux[10], Johanna M. Vos[11], Adam C. Schneider[12], Aaron M. Meisner[13], Caroline Morley[14], J. Davy Kirkpatrick[15], Federico Marocco[15], Rocio Kiman[16], Charles A. Beichman[15], Ben Burningham[17], Dan Caselden[1], Peter R. Eisenhardt[18], Christopher R. Gelino[15], Ehsan Gharib-Nezhad[19], Marc J. Kuchner[20], Brianna Lacy[14], Austin Rothermich[1,2], Melanie J. Rowland[14], and Niall Whiteford[1]
[1] Department of Astrophysics, American Museum of Natural History, New York, NY, USA; sherelyna12@gmail.com
[2] Department of Physics, Graduate Center, City University of New York, New York, NY, USA
[3] Department of Physics and Astronomy, Hunter College, City University of New York, New York, NY, USA
[4] Department of Astronomy & Astrophysics, UC San Diego, La Jolla, CA, USA
[5] Planétarium de Montréal, Montréal, Québec, Canada
[6] Trottier Institute for Research on Exoplanets, Université de Montréal, Département de Physique, Montréal, Québec, Canada
[7] Department of Astronomy and Astrophysics, University of California, Santa Cruz, CA, USA
[8] Department of Physics and Astronomy, San Francisco State University, San Francisco, CA, USA
[9] Department of Physics & Astronomy, Amherst College, Amherst, MA, USA
[10] Department of Theoretical Physics and Astrophysics, Faculty of Science, Masaryk University, Brno, Czech Republic
[11] School of Physics, Trinity College Dublin, The University of Dublin, Dublin, Ireland
[12] United States Naval Observatory, Flagstaff, AZ, USA
[13] NSF National Optical-Infrared Astronomy Research Laboratory, Tucson, AZ, USA
[14] Department of Astronomy, University of Texas at Austin, Austin, TX, USA
[15] IPAC, Caltech, Pasadena, CA, USA
[16] Department of Astronomy, California Institute of Technology, Pasadena, CA, USA
[17] Department of Physics, Astronomy and Mathematics, University of Hertfordshire, Hatfield, UK
[18] NASA Jet Propulsion Laboratory, California Institute of Technology, Pasadena, CA, USA
[19] NASA Ames Research Center, Mountain View, CA, USA
[20] Exoplanets and Stellar Astrophysics Laboratory, NASA Goddard Space Flight Center, Greenbelt, MD, USA
Received 2025 March 17; revised 2025 May 29; accepted 2025 May 29; published 2025 August 5

Abstract

We present a near-complete spectral energy distribution (SED) for an extrasolar world: the T8 brown dwarf 2MASS J04151954−0935066. Spanning from optical to mid-infrared (0.7–20.4 μm) wavelengths, the SED for this substellar atmosphere is constructed from new James Webb Space Telescope (JWST) NIRSpec G395H ($R \sim 2700$) and Magellan Folded-port InfraRed Echellete (FIRE) echelle ($R \sim 8000$) near-infrared spectra, along with MIRI mid-infrared photometry complemented by spectra from Keck I, Infrared Telescope Facility, Magellan, AKARI, Spitzer, and photometry from various surveys and missions. The NIRSpec G395H spectrum reveals strong molecular absorptions from NH_3, CH_4, H_2S, CO_2, and H_2O at approximately 3.00, 3.35, 3.95, 4.25, and 5.00 μm, respectively, along with the presence of a CO absorption feature detected mainly at ∼4.6 μm. We detect no absorption of near-infrared K I doublets in the $R \sim 8000$ FIRE spectra. In the mid-infrared Infrared Spectrograph spectrum, we tentatively identify a new CO_2 feature at 14–16 μm. The comprehensive SED allows us to empirically constrain bolometric luminosity, effective temperature, mass, and radius. Additionally, we demonstrate that the NIRSpec G395H resolution, the highest allowable by JWST, enables a precise radial velocity measurement of 47.1 ± 1.8 km s^{-1} for the object, in agreement with previous measurements.

Unified Astronomy Thesaurus concepts: Brown dwarfs (185)

Materials only available in the online version of record: data behind figure

1. Introduction

The observations of Teide 1 (R. Rebolo et al. 1995) and the cold companion Gl 229B (T. Nakajima et al. 1995; B. R. Oppenheimer et al. 1995) were the first detections of brown dwarfs. With their discoveries, substellar-mass physics began bridging the gap in our understanding between low-mass stars and giant Jovian worlds like those found in our solar system. Brown dwarfs (objects with masses $<\sim 75 M_{\rm Jup}$) were theorized in the 1960s (S. S. Kumar 1963) but required advancements in infrared surveys (e.g., the Two-Micron All-Sky Survey, or 2MASS; R. M. Cutri et al. 2003) in order to be found in large quantities. Brown dwarfs range in temperature from ∼3000 K through ∼250 K (e.g., J. D. Kirkpatrick et al. 2024), which correspond to the spectral classes of late-type M, L, T, and Y dwarfs (E. L. Martín et al. 1999; J. D. Kirkpatrick et al. 1999; A. J. Burgasser et al. 2002; M. C. Cushing et al. 2011). Because the temperatures differ across spectral class, the atmospheric chemistry and hence molecular absorption in the observed data of brown dwarfs changes with spectral subtype. For T-type dwarfs, water (H_2O), methane (CH_4), and ammonia (NH_3) gases can dominate the infrared. Strong

abundances of CO and CO_2 are also found in a variety of characterized T dwarfs (e.g., I. Yamamura et al. 2010; B. E. Miles et al. 2020; S. Mukherjee et al. 2022), which suggests an atmosphere in disequilibrium chemistry due to strong vertical mixing (B. R. Oppenheimer et al. 1995; J. Fegley Bruce & K. Lodders 1996; C. A. Griffith & R. V. Yelle 1999).

The majority of brown dwarf spectroscopic follow-up observations through the early 21st century were done with ground-based facilities in the near-infrared (e.g., A. J. Burgasser et al. 2004, J. D. Kirkpatrick et al. 2011, 2010) which covered ∼1–2.5 μm. However, the 3–5 μm spectral window contains critical coverage of CH_4, H_2O, NH_3, and bands of CO and CO_2 for brown dwarfs. Unfortunately, observations of this spectral region are challenging from the ground due to the brightness of the Earth's atmosphere. Fortunately, space missions like AKARI collected spectroscopic observations probing this region of interest (H. Murakami et al. 2007), furthering our understanding of exoplanets and brown dwarf atmospheres. The launch of the space-based infrared observatory the James Webb Space Telescope (JWST) enabled the continuation of these studies at a greater sensitivity (J. Rigby et al. 2023). For instance, B. E. Miles et al. (2023) presented a high-fidelity 1–20 μm spectrum of the planetary companion late-type L dwarf VHS J125601.92−125723.9 obtained with JWST. They illustrated how disequilibrium chemistry impacts the spectral shape, in addition to a vast array of molecular species.

Discovered in A. J. Burgasser et al. (2002), the T8 dwarf 2MASS J04151954−0935066 (2MASS J0415−0935 for short) has been the subject of several thorough studies, and it is a standard for spectral classification of late-type, cool T dwarfs (e.g., S. K. Leggett et al. 2007; D. Saumon et al. 2007; I. Yamamura et al. 2010; B. E. Miles et al. 2020; C. E. Hood et al. 2024). Characterizing this object with additional, detailed JWST observations will solidify its use as a benchmark brown dwarf as it can be used to ground atmospheric models and comparative surveys of lesser known sources.

In this paper, we present new near- and mid-infrared observations for 2MASS J0415−0935 complemented with archival ground- and space-based observations which yield a near-complete (0.7–20.4 μm) spectral energy distribution (SED) of an extrasolar atmosphere covering 93% of its total bolometric luminosity. The data analyzed herein precisely constrain the luminosity and effective temperature for 2MASS J0415−0935. There are only a handful of similarly complete SEDs of brown dwarfs reported in the literature to date, including (i) the aforementioned 0.97–19.8 μm SED for VHS 1256 B in B. E. Miles et al. (2023), which used JWST NIRSpec and MIRI spectroscopic observations, and (ii) the 0.8–15 μm SED for HN Peg B from G. Suárez et al. (2021), which is composed of data from various space- and ground-based facilities.

In Section 2, we present optical to mid-infrared spectrophotometry for 2MASS J0415−0935. In Section 3, we discuss the process of constructing the SED, how fundamental parameters were derived, and analyze the values in context with all known brown dwarfs. Additionally, we detail what is extracted from the data including kinematics and molecular features. Conclusions are presented in Section 4.

2. Observations and Data Reduction

2MASS J0415−0935 has both new and archived data, which are both discussed in detail in this section. All data are available for download from the SIMPLE Archive,[21] a repository for data related to brown dwarfs, directly imaged exoplanets, and low-mass stars.

2.1. New Data

We present new data for 2MASS J0415−0935 acquired from the Magellan telescope and through the JWST Cycle 1 GO #2124 program (PI: J. Faherty).

2.1.1. Magellan/FIRE Echellete Spectrum

During 2010 September 20 (UT), we acquired near-infrared spectroscopic observations of 2MASS J0415−0935 using the Folded-port InfraRed Echellete (FIRE) spectrograph on the 6.5 m Baade Magellan telescope (R. A. Simcoe et al. 2013). Observing conditions were clear with 0.″5 seeing. We used echellete mode and a 0.″6 slit with 2 × 900 s exposures (AB) at an average air mass of 1.063. The A0 V star HD 31004 was observed for flux calibration. The data were reduced using the FIREHOSE pipeline, which is based on the MASE and Spextool reduction packages (W. D. Vacca et al. 2003; M. C. Cushing et al. 2004; J. J. Bochanski et al. 2009).[22] The resulting spectrum has a wavelength coverage of 0.8–2.5 μm with a resolution of $R \sim 8000$, and is shown in Figure 1.

2.1.2. JWST/NIRSpec G395H Medium-resolution Spectroscopy

NIRSpec data for 2MASS J0415−0935 were obtained on 2022 October 16 using the F290LP filter, the G395H grating, the S200A1 aperture, and the SUB2048 subarray. Acquisition images were first obtained for each target using the WATA method, the CLEAR filter, and the NRSRAPID readout pattern. We used 11 groups per integration, three integrations per exposure, and three total dithers for a summation of nine total integrations in 168.488 s of exposure time.

For the reduction of the NIRSpec G395H spectra, we ran the JWST calibration pipeline v1.10.0 (H. Bushouse et al. 2023), using the Calibration Reference Data System context file jwst_1146.pmap and default parameters. We optimized the aperture extraction considering the slit position of the target. The resulting combined spectrum has a wavelength coverage that ranges from 2.87 to 5.14 μm with a resolution of ∼2700, and is shown in Figure 2.

2.1.3. JWST MIRI Photometry

MIRI photometry was obtained on 2022 September 18 with the F1000W (9.023–10.891 μm), F1280W (11.588–14.115 μm), and F1800W (16.519–19.502 μm) filters. For each filter the FASTR1 readout pattern was chosen with a two-point dither pattern. 2MASS J0415−0935 was observed with MIRI using five groups per integration for each filter. The total exposure time plus overhead for the MIRI observing of 2MASS J0415−0935 was 0.52 hr.

We used the MIRI photometry provided by the JWST pipeline, which agrees well with the existing Spitzer Infrared Spectrograph (IRS) spectrum. We calculated synthetic

[21] http://simple-bd-archive.org/

[22] https://wikis.mit.edu/confluence/display/FIRE/FIRE+Data+Reduction

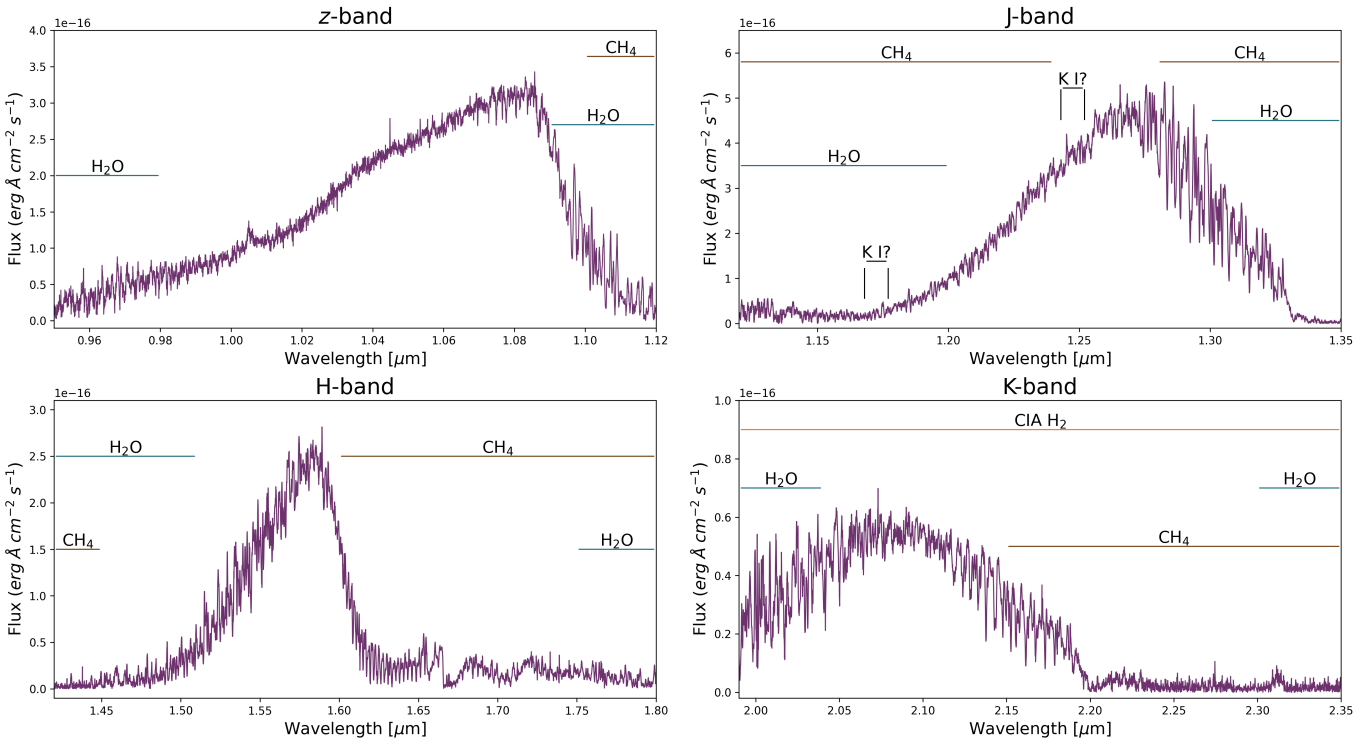

Figure 1. Magellan FIRE spectrum with panels showing the z-band, J-band, H-band, and K-band regions along with prominent molecular absorption from CH_4 and H_2O.

F1000W, F1280W, and F1800W fluxes from the Spitzer/IRS spectrum. The flux differences between the MIRI photometry and IRS synthetic fluxes are well within the uncertainties (1.703 ± 0.022 mJy, 1.393 ± 0.038 mJy, and 0.708 ± 0.264 mJy) in the F1000W, F1280W, and F1800W filters, respectively. The IRS spectrum does not fully cover the F1800W filter, so the reported flux difference is an upper value. The MIRI and NIRSpec data can be obtained from the Mikulski Archive for Space Telescopes at the Space Telescope Science Institute via doi:10.17909/g9r5-0q61.

2.2. Literature Data

In order to construct the SED of 2MASS J0415−0935, we complemented the new data with previously published data which are publicly available in the SIMPLE Archive.

2.2.1. Keck I/LRIS Spectrum

A. J. Burgasser et al. (2003) observed 2MASS J0415−0935 with the Low Resolution Imaging Spectrometer (LRIS) mounted on the Keck I 10 m telescope (J. B. Oke et al. 1995), spanning the 0.63–1.01 μm wavelength range with a resolution of $R \sim 1000$.

2.2.2. IRTF/SpeX Spectrum

A. J. Burgasser et al. (2004) published a near-infrared (0.8–2.5 μm), low-resolution ($R \sim 150$) spectrum of 2MASS J0415−0935, observed using the SpeX spectrograph mounted on the Infrared Telescope Facility (IRTF) on Maunakea, HI (J. T. Rayner et al. 2003). 2MASS J0415−0935 was designated as a late-T spectral standard and consequently aided in the classification of subsequent T dwarf discoveries.

2.2.3. AKARI/IRC Spectrum

I. Yamamura et al. (2010) published mid-infrared spectroscopic observations of L1–T8 dwarfs with the InfraRed Camera from the AKARI mission (H. Murakami et al. 2007) with a wavelength coverage of 2.5–5 μm and a spectral resolution of $R \sim 120$. 2MASS J0415−0935 was one of the targets published with AKARI data. I. Yamamura et al. (2010) examined the strength of molecular absorption bands from CH_4 at 3.3 μm, CO_2 at 4.2 μm, and CO at 4.6 μm.

2.2.4. Spitzer/IRS Spectrum

G. Suárez & S. Metchev (2022) reprocessed a mid-infrared (5.2–20 μm), low-resolution ($R \sim 100$) spectrum of 2MASS J0415−0935 obtained with the IRS on the Spitzer Space Telescope (J. R. Houck et al. 2004), originally published in D. Saumon et al. (2007).

2.2.5. Literature Photometric Observations

There are a number of publicly available photometric observations for 2MASS J0415−0935 that also contribute to the SED. For optical photometry, magnitudes published in S. K. Leggett et al. (2012) for the i and z filters from the Sloan Digital Sky Survey (SDSS; D. G. York et al. 2000) were used. Offsets from P. C. Hewett et al. (2006) were implemented to convert values from the AB to Vega system. For near-infrared photometry, we used data from 2MASS, the VHS Data Release 6, and the UKIRT Fast-Track Imager on the United Kingdom Infrared Telescope (G. R. Knapp et al. 2004; N. Lodieu et al. 2012; D. A. Golimowski et al. 2004). The latter uses the Maunakea Observatory filters. Additionally, photometry in the three F090M, F110W, and F170M filters from the Near Infrared Camera and Multi-Object Spectrometer

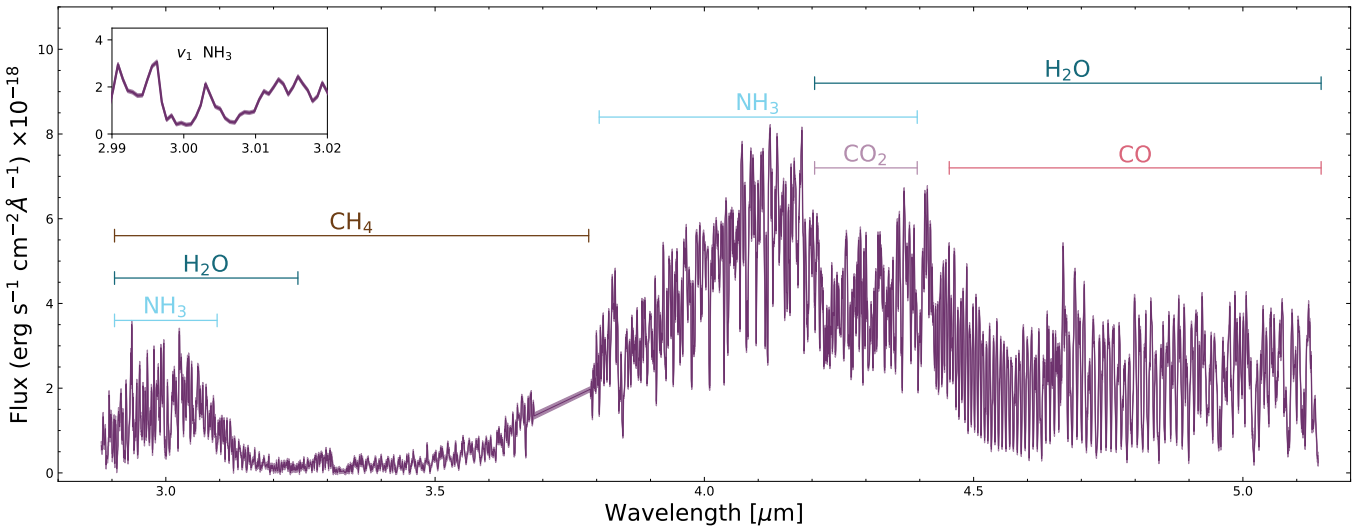

Figure 2. JWST/NIRSpec G395H spectrum for 2MASS J0415−0935 with the uncertainties in the shaded region. The inset plot displays a zoom-in to the v_1 NH_3 band.

on the Hubble Space Telescope (HST) published in A. J. Burgasser et al. (2006b) was included. Photometry at 3.6 μm (ch1), 4.5 μm (ch2), 5.7 μm (ch3), and 7.8 μm (ch4) from the InfraRed Array Camera on the Spitzer Space Telescope was also included (B. M. Patten et al. 2006). Mid-infrared magnitudes from the Wide Field Infrared Survey Explorer (WISE) were also included. WISE W1 and W2 band photometry were taken from the CatWISE2020 catalog (F. Marocco et al. 2021), while the W3 and W4 bands were from AllWISE (R. M. Cutri et al. 2013). All these observations are listed in Table 1.

3. Spectral Energy Distribution and Fundamental Parameters of 2MASS J0415–0935

3.1. Constructing the SED

The open-source Python package SEDkit V.2.0.5[23] (J. Filippazzo et al. 2024) was used in order to facilitate the construction of the SED shown in Figure 3. SEDkit was used to calculate a precise bolometric luminosity ($L_{\rm bol}$) and semi-empirically determine effective temperature along with other fundamental parameters. It was modified to include a Monte Carlo approach (Section 3.2) during calculations to work in conjunction with an open-source python wrapper called SEDkitSIMPLE.[24] The wrapper was developed to automate the process of loading data from the SIMPLE Archive into SEDkit.

The process of SED construction was as follows:

1. We used SEDkit to call SIMPLE and load the spectra and photometry presented in Section 2.
2. The published effective wavelengths for each filter were determined assuming a Vega spectrum (C. Rodrigo & E. Solano 2020). In order to better represent these photometry values in the context of the entire SED, we calculated the effective wavelengths using the actual spectra of 2MASS J0415−0935. These effective wavelengths are used to plot the photometry points shown in Figure 3 and are included as Data Behind the Figure (DbF).
3. Spectra with overlapping regions are shown in Figure 4. With the exception of the AKARI and NIRSpec spectra,

Table 1
Photometry of 2MASS J0415−0935

Band	Vega Magnitude	References
SDSS i	23.084 ± 0.090	L12
SDSS z	18.867 ± 0.090	L12
2MASS J	15.695 ± 0.058	C03
2MASS H	15.537 ± 0.113	C03
2MASS K_S	15.429 ± 0.201	C03
VHS Y	16.451 ± 0.008	VDR6
VHS J	15.327 ± 0.004	VDR6
VHS H	15.680 ± 0.012	VDR6
VHS K_S	15.683 ± 0.023	VDR6
MKO J	15.32 ± 0.03	K04
MKO H	15.70 ± 0.03	K04
MKO K	15.83 ± 0.03	K04
MKO L'	13.28 ± 0.05	G04
MKO M'	12.82 ± 0.15	G04
HST F090M	19.04 ± 0.10	B06
HST F110W	16.47 ± 0.05	B06
HST F170M	16.67 ± 0.06	B06
WISE W1	15.148 ± 0.026	M21
WISE W2	12.305 ± 0.011	M21
WISE W3	11.132 ± 0.113	C13
WISE W4	>8.638	C13
Spitzer [3.6]	14.256 ± 0.019	K19
Spitzer [4.5]	12.374 ± 0.017	K19
Spitzer [5.7]	12.87 ± 0.070	P06
Spitzer [7.8]	12.11 ± 0.050	P06
JWST F1000W	10.749 ± 0.002	TW
JWST F1280W	10.669 ± 0.002	TW
JWST F1800W	10.327 ± 0.007	TW

References. (C03) R. M. Cutri et al. (2003); (D12) T. J. Dupuy & M. C. Liu (2012); (H21) C.-C. Hsu et al. (2021); (B03) A. J. Burgasser et al. (2003); (L12) S. K. Leggett et al. (2012); (VDR6) VHS Data Release 6; (B21) W. M. J. Best et al. (2021); (K04) G. R. Knapp et al. (2004); (G04) D. A. Golimowski et al. (2004); (B06) A. J. Burgasser et al. (2006b); (M21) F. Marocco et al. (2021); (C13) R. M. Cutri et al. (2013); (K19) J. D. Kirkpatrick et al. (2019); (P06) B. M. Patten et al. (2006); (TW) this work.

[23] V.2.0.5 of SEDkit fixed bugs in previous versions related to uncertainties in the fundamental parameters and calculations of the absolute magnitudes.
[24] https://github.com/dr-rodriguez/SEDkitSIMPLE

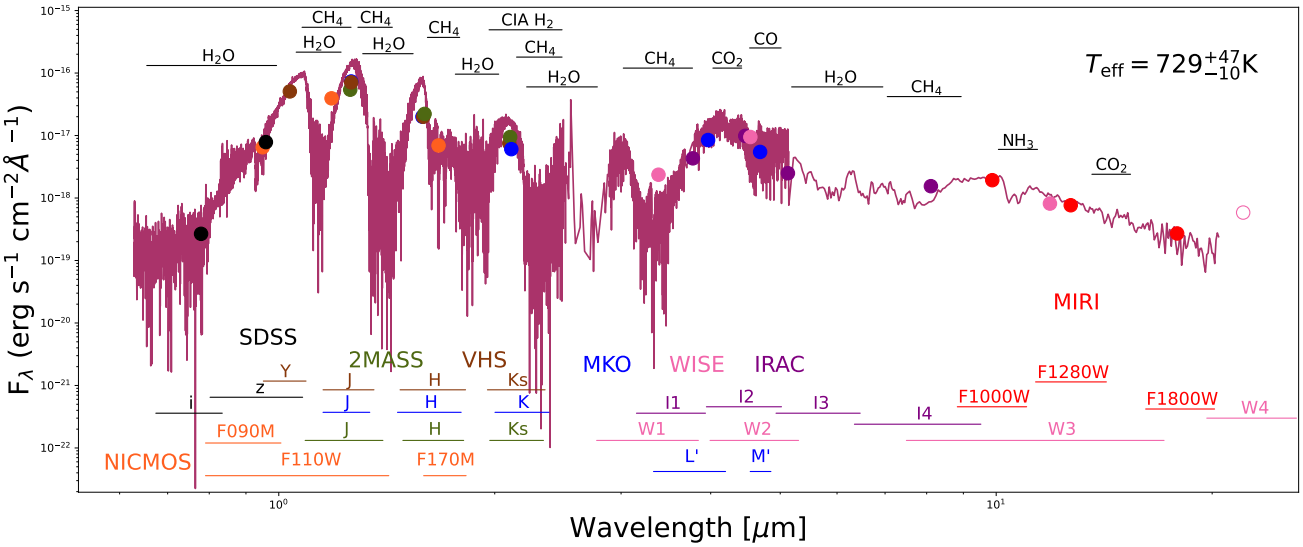

Figure 3. Distance-calibrated SED of 2MASS J0415−0935 using new JWST NIRSpec and MIRI observations and spectrophotometry from the literature, as indicated in the plot. We label the principal molecular bands for H_2O, CH_4, CIA H_2, NH_3, and CO along with the calculated $T_{\rm eff}$ of the object. The photometry used is denoted by circles in the same corresponding color to the filters shown at the bottom of the plot, and the circles are centered at the effective wavelength of each filter, which were obtained using the SED for 2MASS J0415−0935. The flux densities, wavelengths, and photometry used to generate this figure are available.
(The data used to create this figure are available in the online article.)

overlapping spectra were combined by smoothing the higher signal-to-noise ratio (SNR) spectrum to the lowest-resolution wavelength array and then normalized following J. C. Filippazzo et al. (2015). In the 2.9–5 μm region, the AKARI spectrum was trimmed to give preference to the JWST observations.

4. The spectra and photometry were distance-scaled using a parallax of 175.2 ± 1.7 mas (T. J. Dupuy & M. C. Liu 2012).
5. SEDkit constructed the distance-scaled flux-calibrated SED of our object by starting at zero in wavelength and then linearly interpolating to the shortest-wavelength data point (0.7 μm), continuing with the observations, and then appending a Rayleigh–Jeans tail from the longest available wavelength data point at 20.4 μm up to 1000 μm. The flux from the SED shown in Figure 3 was integrated to provide a measurement of the $L_{\rm bol}$.
6. In order to calculate the effective temperature ($T_{\rm eff}$) using the Stefan–Boltzmann law and the calculated $L_{\rm bol}$, a radius is required. We estimated a radius using the best age approximation and the solar-metallicity, hybrid cloud evolutionary model isochrones from D. Saumon & M. S. Marley (2008). 2MASS J0415−0935 shows no signs of low gravity nor low metallicity, but rather has kinematics consistent with a field age brown dwarf (see, e.g., C.-C. Hsu et al. 2021, C. E. Hood et al. 2024). Therefore, we assumed a broad age range of 0.5–8.5 Gyr to semi-empirically extract all other fundamental parameters.
7. SEDkit returns a SED for 2MASS J0415−0935 and all fundamental parameters.

All parameters calculated are presented in Table 2, and the distance-calibrated SED is shown in Figure 3.

3.2. Monte Carlo Approach for Uncertainty Estimates

The V.2.0.5 of SEDkit used a Monte Carlo approach to derive model-dependent fundamental parameters and uncertainties. This Monte Carlo approach used the given age range of the object along with the calculated $L_{\rm bol}$ and its uncertainty. It then generated a Gaussian distribution for bolometric luminosity using the $L_{\rm bol}$ value as the peak and its uncertainty as the standard deviation. For the age distribution of the object, we assumed a uniform distribution between the lowest (0.5 Gyr) and highest (8.5 Gyr) end of our adopted age range. We sampled 10^4 values from these distributions and combined each $L_{\rm bol}$–age pair into the evolutionary models to acquire M, R, and $\log g$ values. We then considered the 68% confidence interval as the uncertainties on the model-dependent parameters, and took the median as the parameter values provided.

3.3. Analysis of Fundamental Parameters

Comparing the fundamental parameter values listed in Table 2 to those in previous results, namely C. E. Hood et al. (2024), J. A. Zalesky et al. (2022), J. C. Filippazzo et al. (2015), D. Saumon et al. (2007), A. J. Burgasser et al. (2006a), F. J. Vrba et al. (2004), and D. A. Golimowski et al. (2004), we find they generally agree within 2σ. For instance, the work presented in J. C. Filippazzo et al. (2015) used the same method of determining fundamental parameters described in Section 3.1—excluding the aforementioned changes to the code—making it a good comparison point. Nonetheless, there are several differences that are of importance to note, including a change in parallax measurement and an addition of mid-infrared spectra (AKARI, JWST, and Spitzer) and photometry (VHS, HST, and MIRI). The $L_{\rm bol}$ from this paper is slightly larger than the calculated value in J. C. Filippazzo et al. (2015) although it is within 3σ. Similarly, our $T_{\rm eff}$ is within 1σ from J. C. Filippazzo et al. (2015), yet it is slightly warmer given that our SED has mid-infrared observations missing from the J. C. Filippazzo et al. (2015) analysis.

The work from C. E. Hood et al. (2024) conducts a spectral inversion analysis of this source and makes use of the SED presented in this paper exclusive of the Magellan, LRIS, and

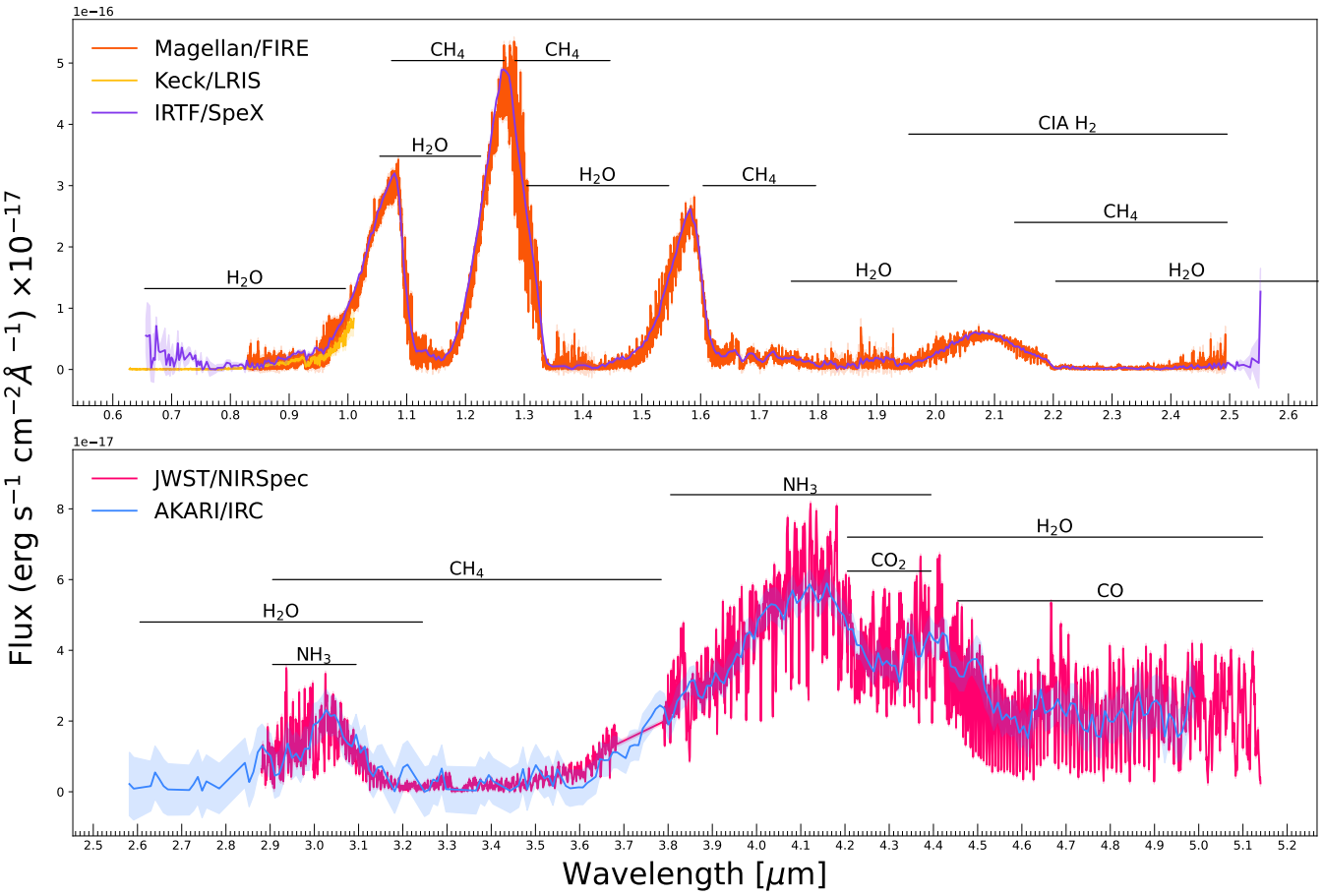

Figure 4. Top panel: spectra from Magellan/FIRE (orange), Keck/LRIS (yellow), and IRTF/SpeX (purple). Bottom panel: spectra from JWST/NIRSpec (pink) and AKARI/IRC (blue). Shaded regions represent the flux uncertainties of each individual spectrum. The main spectral features are indicated.

Table 2
Fundamental Parameters of 2MASS J0415−0935

Parameter	Value	Unit
$\log(L_{\rm bol}/L_{\odot})$	$-5.71^{+0.01}_{-0.01}$	...
$T_{\rm eff}$	729^{+47}_{-10}	K
Radius	$0.855^{+0.110}_{-0.020}$	$R_{\rm Jup}$
Mass	37^{+10}_{-12}	$M_{\rm Jup}$
$\log g$	$5.13^{+0.12}_{-0.35}$	dex

AKARI spectra, making it the most comparable. As noted in C. E. Hood et al. (2024), the retrieved fundamental parameters are within 1σ of the SED analysis, with the exception of their smaller radius, which is 3σ lower than our results. This difference is noted by C. E. Hood et al. (2024) as being a standard problem in brown dwarf retrieval studies.

Other works like those presented in F. J. Vrba et al. (2004) introduced a $T_{\rm eff}$ of 764^{+88}_{-71} K for 2MASS J0415−0935, which is within 1σ of our work. By using their $M_{\rm bol}$ estimate of 18.70 ± 0.26 mag, they derived an $L_{\rm bol}$ of $-5.58 \pm 0.10\ L_{\odot}$, which is within 2σ from our results. Similarly, D. A. Golimowski et al. (2004) presented a range of 600–700 K for the $T_{\rm eff}$ of 2MASS J0415−0935 based on a parallax measurement plus near-infrared spectra and photometry. The limited spectral coverage resulted in a temperature 3σ cooler than our results. These comparisons demonstrate the need for full spectral coverage to account for substellar object flux and precisely measure fundamental parameters.

The observed and estimated properties of 2MASS J0415−0935 are provided in Table 2.

3.4. Radial Velocity

With the high resolution of the G395H spectra, we were able to calculate a radial velocity for 2MASS J0415−0935. We used a forward-model sampling method with Markov Chain Monte Carlo using four parameters (radial velocity, line-spread function width, two blaze parameters) on many segments of the spectrum, adopting the segments with the most stable and reproducible radial velocities in each model grid. In our approach we compared to the B. Lacy & A. Burrows (2023) models, the Elf Owl models from S. Mukherjee et al. (2024), and the C. V. Morley et al. (2012) models. We obtained a radial velocity measurement for 2MASS J0415−0935 of 47.1 ± 1.8 km s^{-1}. Our results are within 2σ from the radial velocity of 51.1 ± 1.8 km s^{-1} published in C.-C. Hsu et al. (2021) using Keck NIRSPEC data.

3.5. Kinematic Analysis

Using the proper motion, parallax, and radial velocity, we calculated component velocities for 2MASS J0415−0935. We found U, V, and W values of −63 ± 1.0, −42.4 ± 0.6, and 17 ± 1.0 km s^{-1}, respectively, with a total velocity of 77.8 ± 1.5 km s^{-1}. Using the BANYAN Σ tool (J. Gagné et al. 2018),

Table 3
Astrometric and Kinematic properties of 2MASS J0415−0935

Parameter	Value	Units	References
R.A. (J2000)	04:15:19.54008	⋯	C03
Decl. (J2000)	−09:35:06.6012	⋯	C03
$\mu_\alpha \cos\delta$	2214.3 ± 1.2	mas yr^{-1}	D12
μ_δ	535.9 ± 1.2	mas yr^{-1}	D12
Parallax	175.2 ± 1.7	mas	D12
$v \sin i$	33.5 ± 2.0	km s^{-1}	H21
X	−4.09 ± 0.04	pc	TW
Y	−1.73 ± 0.02	pc	TW
Z	−3.59 ± 0.03	pc	TW
U	−63 ± 1.00	km s^{-1}	TW
V	−42.4 ± 0.60	km s^{-1}	TW
W	17.0 ± 1.00	km s^{-1}	TW
Radial velocity	47.1 ± 1.80	km s^{-1}	TW
Total velocity	77.8 ± 1.50	km s^{-1}	TW

References. (C03) R. M. Cutri et al. (2003); (D12) T. J. Dupuy & M. C. Liu (2012); (H21) C.-C. Hsu et al. (2021); (B03) A. J. Burgasser et al. (2003); (L12) S. K. Leggett et al. (2012); (VDR6) VHS Data Release 6; (B21) W. M. J. Best et al. (2021); (K04) G. R. Knapp et al. (2004); (G04) D. A. Golimowski et al. (2004); (B06) A. J. Burgasser et al. (2006b); (M21) F. Marocco et al. (2021); (C13) R. M. Cutri et al. (2013); (K19) J. D. Kirkpatrick et al. (2019); (P06) B. M. Patten et al. (2006); (TW) this work.

we input all astrometric parameters and evaluated if 2MASS J0415−0935 shows any kinematic correlation with a known moving group or association. BANYAN Σ revealed a 99.9% field population probability, reaffirming that it is a field dwarf.

3.6. Spectral Features

Within this section we describe the spectral features we observed in 2MASS J0415−0935.

3.6.1. Optical

The optical portion of the SED was previously published in the work of A. J. Burgasser et al. (2003). The LRIS spectrum displays molecular absorption features such as FeH, CrH, K I, and H_2O. A. J. Burgasser et al. (2003) also found an absence of any Li I absorption in 2MASS J0415−0935. This might be due to the lower SNR of the optical data or a very small absorption abundance of Li I in this object. To date only a few T dwarfs have yielded a Li I detection (J. K. Faherty et al. 2014; J. S. Pineda et al. 2016; E. L. Martín et al. 2022).

3.6.2. Near-infrared and Mid-infrared

Typically, near-infrared spectroscopic observations of T dwarfs are demarcated by the presence of H_2O and CH_4 in the *J*, *H*, and *K* bands, along with collision-induced absorption (CIA) due to H_2 in the *K* band (S. K. Leggett et al. 2000; A. J. Burgasser et al. 2002; B. E. Miles et al. 2020). In Figure 1, the *z*, *J*, *H*, and *K* bands from the FIRE spectrum are displayed. Absorption features from CH_4 and H_2O are labeled in the *z*-band (0.95–1.12 μm) panel. In the *J*-band (1.12–1.35 μm) panel, absorption features from H_2O and CH_4 are clearly identified. The location of the K I doublet at 1.243/1.252 and 1.168/1.177 μm is labeled, but not detected in the $R \sim 8000$ FIRE spectrum for this late-T dwarf. Given the median SNR of ∼98 in this region and the overall resolution of $R \sim 8000$, the K I doublet should be detectable if present, but it is absent. Like the previous two bands, in the *H* band (1.45–1.80 μm) CH_4 absorption is prominent. Lastly, the *K* band (2.0–2.35 μm) is marked by the presence of CIA H_2, H_2O, and CH_4. A CO absorption band centered at 2.3 μm is commonly observed in warmer M, L, and early-T dwarfs (S. K. Leggett et al. 2000; A. J. Burgasser et al. 2002), however it is not present in 2MASS J0415−0935. As has been found in late-type T dwarfs, CH_4 absorption overpowers this region of the spectrum.

The JWST/NIRSpec spectrum shown in Figure 2 displays notable features from H_2O, CH_4, CO_2 and CO. A strong CO feature at 4.6–5.0 μm clearly demonstrates the CO disequilibrium chemistry—which was observed in brown dwarfs with the discovery of Gl 229B (T. Nakajima et al. 1995; B. R. Oppenheimer et al. 1995)—and confirms the result seen in the lower-resolution, lower-SNR AKARI spectrum (I. Yamamura et al. 2010).

Within the NIRSpec spectrum, we find the υ_1 band feature of NH_3 at 3 μm. This feature was tentatively identified for the first time in a cold substellar object in the NIRSpec low-resolution data of the Y0 dwarf WISE J035934.06−540154.6 (S. A. Beiler et al. 2023). In the atmospheric retrieval work of C. E. Hood et al. (2024), a total abundance value of $\log(NH_3) = -5.0^{+0.04}_{-0.03}$ was retrieved using the SpeX prism, JWST/NIRSpec, and Spitzer/IRS spectra. Our visual inspection complemented by the C. E. Hood et al. (2024) value confirms the presence of the NH_3 feature.

To be thorough in our examination, we checked for the presence of lithium chloride (LiCl) in the near- and mid-infrared portions of the SED using abundances from the ExoMol database (J. Buldyreva et al. 2022; E. R. Guest et al. 2024). The work from E. Gharib-Nezhad et al. (2021) predicts LiCl to be the dominant lithium-bearing molecule in an 800K atmosphere, however other molecular species (including CO_2, CH_4, NH_3, and CO) dominate the spectra for the object in this paper. Despite the SNR and resolution of the data, we found no signature of LiCl.

We do, however, tentatively identify a CO_2 feature at 14–16 μm present in the Spitzer/IRS spectrum displayed in Figure 5. All cross sections used for analysis in this work are from the HITRAN high-resolution transmission molecular absorption database (C. Richard et al. 2012; G. Li et al. 2015; R. J. Hargreaves et al. 2020) and the ExoMol database (J. Tennyson & S. N. Yurchenko 2012; C. Sousa-Silva et al. 2015; O. L. Polyansky et al. 2018; P. A. Coles et al. 2019). The JWST photometric measurements at 10, 12.8, and 18 μm as seen in Figure 3 further corroborate the features seen in the spectrum from Spitzer. The cross sections in Figure 5 indicate the presence of water and ammonia in this same wavelength regime, but the narrow feature at 14–16 μm is well aligned with CO_2 absorption. While this υ_2-band CO_2 feature has been observed in stars (e.g., K. Justtanont et al. 1998; N. Ryde et al. 1998), this is the first time it has been identified in a brown dwarf atmosphere. Obtaining higher-resolution spectroscopic observations of cold brown dwarfs in the mid-infrared will allow for better constraints on the existence of this CO_2 feature and whether it is further evidence of disequilibrium chemistry. Predictions of the features observed in our SED using modern atmospheric models will be evaluated in a separate study (G. Suárez et al. 2024, in preparation).

3.7. Flux Calibration Verification

With the flux-calibrated SED for 2MASS J0415−0935, we calculated synthetic photometry to evaluate the absolute flux calibration by the JWST pipeline. In Figure 6, we display the

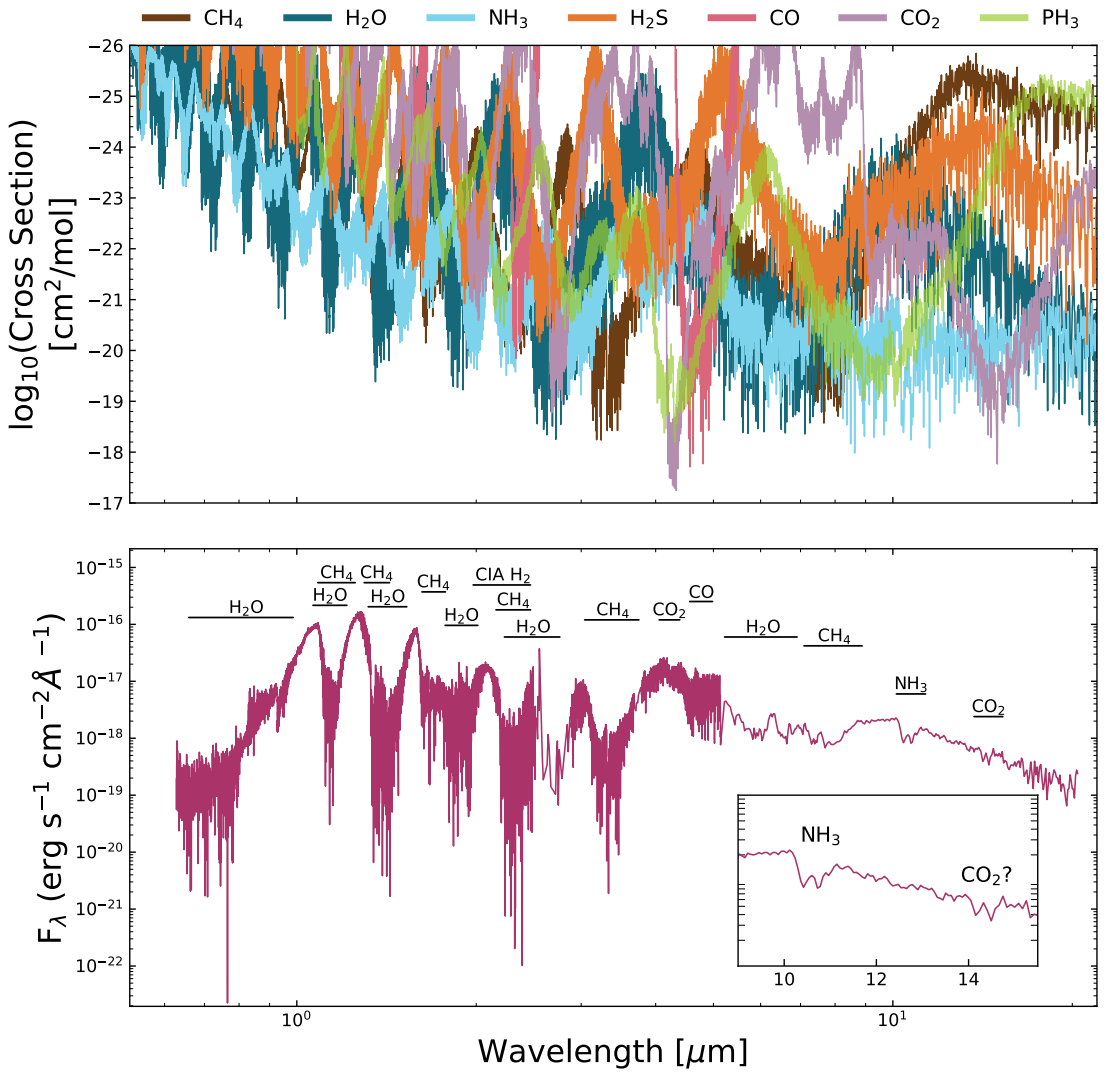

Figure 5. Top panel: absorption cross sections for a temperature of 650 K and pressure of 1 bar used in the retrieval analysis from C. E. Hood et al. (2024). Bottom panel: the complete SED for 2MASS J0415−0935 with an inset showing the 9–15 μm region. Prominent absorption features are labeled, including a tentative CO_2 feature between 14 and 16 μm.

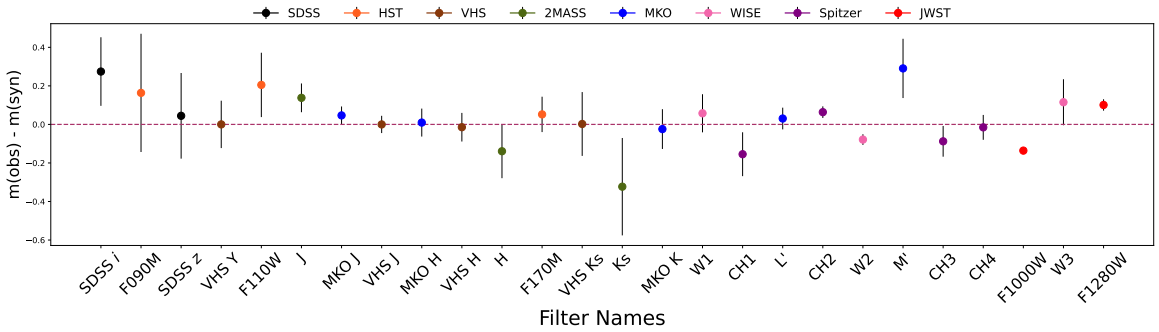

Figure 6. Residuals between observed and synthetic magnitudes from the SED. The different photometric surveys are indicated at the top and the specific filter names are at the bottom. A one-to-one line is indicated by the pink dashed line.

magnitude differences between synthetic and observed photometry from the SED. Overall, the photometric points fit within 1–2σ of the synthetic values with a few exceptions.

The residuals for Spitzer ch1 photometry compared to JWST synthetic points have been noted on other objects in the literature. For instance, in K. L. Luhman et al. (2024) synthetic NIRSpec spectra of WISE J085510.83−071442.5 were compared to the Spitzer ch1 value and found to be significantly discrepant. They also highlighted a comparable divergence in synthetic Spitzer ch1 photometry from the NIRSpec prism spectrum of WISE J035934.06−540154.6 (S. A. Beiler et al. 2023) and its published Spitzer value. Although WISE

J085510.83−071442.5 and WISE J035934.06−540154.6 are cooler Y dwarfs with increased flux in the Spitzer ch2 band, this discrepancy clearly persists in the warmer late-type T dwarfs. Furthermore, S. A. Beiler et al. (2024) corroborated this magnitude difference between synthetic and observed photometry in ch1. After analyzing 23 ultracool dwarfs, they found sources observed by JWST were systematically ∼0.3 mag fainter than the published Spitzer ch1 band when magnitudes were calculated synthetically using NIRSpec prism data.

Also notable in Figure 6 is the comparison between our F1000W magnitude and the synthetic Spitzer/IRS value. The residuals between these two points are ∼0.14 mag (8σ) deviant. This residual is larger than the difference of ∼0.04 mag reported by S. A. Beiler et al. (2024). They tested flux calibration using MIRI low-resolution spectroscopy observations from 5 to 14 μm in the mid-infrared region, whereas we used a Spitzer/IRS spectrum from 5.2 to 20 μm. The larger magnitude deviation in F1000W may be explained by differences between the Spitzer and JWST flux calibration. With upcoming JWST observations of ultracool dwarfs that have been previously observed with Spitzer/IRS, this comparison can be further analyzed.

4. Conclusions

We present new near- and mid-infrared spectrophotometry for the late-T dwarf 2MASS J0415−0935 using JWST and the Magellan telescope. We incorporated literature data to assemble a SED spanning 0.7–20.4 μm, which presents one of the most complete SEDs for a substellar atmosphere, covering 93% of the flux required to calculate $L_{\rm bol}$. Using the SED, we calculated a bolometric luminosity of $-5.71^{+0.01}_{-0.01}$ $L_{\odot}$ and, assuming an age range of 0.5–8.5 Gyr, we derived the following parameters: effective temperature (729^{+47}_{-10} K), mass ($37^{+10}_{-12} M_{\rm Jup}$), radius ($0.855^{+0.110}_{-0.020} R_{\rm Jup}$), and $\log g$ ($5.13^{+0.12}_{-0.35}$ dex). With the JWST/NIRSpec G395H spectrum we confirmed the presence of H_2O, NH_3, CH_4, CO_2, and CO. Additionally, we demonstrated the high-resolution nature of the G395H spectrum allowed for a precise radial velocity measurement of 47.1 ± 1.8 km s^{-1}, consistent with literature values. With the Spitzer/IRS spectrum, we tentatively detected the 14–16 μm CO_2 feature for the first time in a substellar-mass object.

With JWST, we have been able to contextualize past characterizations of 2MASS J0415−0935, and learn more about disequilibrium chemistry in some of the coldest brown dwarfs. The extensive SED presented in this work represents a unique data set to robustly test current atmospheric models to learn about the chemical and physical processes that occur in these atmospheres.

Acknowledgments

S.A.M. was partially funded by the John P. McNulty Foundation for a portion of this project. J.F. acknowledges funding support from JWST-GO-02124.001-A as well as NASA XRP grant No. 80NSSC22K0142 and NSF Award 1909776. This research has made use of the Spanish Virtual Observatory (https://svo.cab.inta-csic.es) project funded by MCIN/AEI/10.13039/501100011033/ through grant No. PID2020-112949GB-I00. J.M.V. acknowledges support from a Royal Society Science Foundation Ireland University Research Fellowship (URF\1\221932). This research has made use of the SVO Filter Profile Service "Carlos Rodrigo," funded by MCIN/AEI/10.13039/501100011033/ through grant No. PID2020-112949GB-I00.

Software: SIMPLE Archive (K. Cruz et al. 2025), SEDkit (J. Filippazzo et al. 2024), Astropy (Astropy Collaboration et al. 2022), SVO Filters (C. Rodrigo & E. Solano 2020).

ORCID iDs

Sherelyn Alejandro Merchan https://orcid.org/0000-0003-0548-0093
Jacqueline K. Faherty https://orcid.org/0000-0001-6251-0573
Genaro Suárez https://orcid.org/0000-0002-2011-4924
Kelle L. Cruz https://orcid.org/0000-0002-1821-0650
Adam J. Burgasser https://orcid.org/0000-0002-6523-9536
Jonathan Gagné https://orcid.org/0000-0002-2592-9612
Callie E. Hood https://orcid.org/0000-0003-1150-7889
Eileen C. Gonzales https://orcid.org/0000-0003-4636-6676
Daniella C. Bardalez Gagliuffi https://orcid.org/0000-0001-8170-7072
Jolie L'Heureux https://orcid.org/0009-0009-3024-5846
Johanna M. Vos https://orcid.org/0000-0003-0489-1528
Adam C. Schneider https://orcid.org/0000-0002-6294-5937
Aaron M. Meisner https://orcid.org/0000-0002-1125-7384
Caroline Morley https://orcid.org/0000-0002-4404-0456
J. Davy Kirkpatrick https://orcid.org/0000-0003-4269-260X
Federico Marocco https://orcid.org/0000-0001-7519-1700
Rocio Kiman https://orcid.org/0000-0003-2102-3159
Charles A. Beichman https://orcid.org/0000-0002-5627-5471
Ben Burningham https://orcid.org/0000-0003-4600-5627
Dan Caselden https://orcid.org/0000-0001-7896-5791
Christopher R. Gelino https://orcid.org/0000-0001-5072-4574
Ehsan Gharib-Nezhad https://orcid.org/0000-0002-4088-7262
Marc J. Kuchner https://orcid.org/0000-0002-2387-5489
Brianna Lacy https://orcid.org/0000-0002-9420-4455
Austin Rothermich https://orcid.org/0000-0003-4083-9962
Melanie J. Rowland https://orcid.org/0000-0003-4225-6314
Niall Whiteford https://orcid.org/0000-0001-8818-1544

References

Astropy Collaboration, Price-Whelan, A. M., Lim, P. L., et al. 2022, ApJ, 935, 167
Beiler, S. A., Cushing, M. C., Kirkpatrick, J. D., et al. 2023, ApJL, 951, L48
Beiler, S. A., Cushing, M. C., Kirkpatrick, J. D., et al. 2024, ApJ, 973, 107
Best, W. M. J., Liu, M. C., Magnier, E. A., & Dupuy, T. J. 2021, AJ, 161, 42
Bochanski, J. J., Hennawi, J. F., Simcoe, R. A., et al. 2009, PASP, 121, 1409
Buldyreva, J., Yurchenko, S. N., & Tennyson, J. 2022, RASTI, 1, 43
Burgasser, A. J., Burrows, A., & Kirkpatrick, J. D. 2006a, ApJ, 639, 1095
Burgasser, A. J., Kirkpatrick, J. D., Brown, M. E., et al. 2002, ApJ, 564, 421
Burgasser, A. J., Kirkpatrick, J. D., Cruz, K. L., et al. 2006b, ApJS, 166, 585
Burgasser, A. J., Kirkpatrick, J. D., Liebert, J., & Burrows, A. 2003, ApJ, 594, 510
Burgasser, A. J., McElwain, M. W., Kirkpatrick, J. D., et al. 2004, AJ, 127, 2856
Bushouse, H., Eisenhamer, J., Dencheva, N., et al. 2023, JWST Calibration Pipeline v1.10.0, Zenodo, doi:10.5281/zenodo.7795697
Coles, P. A., Yurchenko, S. N., & Tennyson, J. 2019, MNRAS, 490, 4638
Cruz, K., Rodriguez, D., Alejandro, S., et al. 2025, SIMPLE-AstroDB/SIMPLE-db v1.1.2025.1, Zenodo, doi:10.5281/zenodo.14610862
Cushing, M. C., Kirkpatrick, J. D., Gelino, C. R., et al. 2011, ApJ, 743, 50
Cushing, M. C., Vacca, W. D., & Rayner, J. T. 2004, PASP, 116, 362

Cutri, R. M., Skrutskie, M. F., van Dyk, S., et al. 2003, 2MASS All Sky Catalog of Point Sources (NASA/IPAC Infrared Science Archive), http://irsa.ipac.caltech.edu/applications/Gator/
Cutri, R. M., Wright, E. L., Conrow, T., et al. 2013, Explanatory Supplement to the AllWISE Data Release Products, http://wise2.ipac.caltech.edu/docs/release/allwise/expsup/index.html
Dupuy, T. J., & Liu, M. C. 2012, ApJS, 201, 19
Faherty, J. K., Beletsky, Y., Burgasser, A. J., et al. 2014, ApJ, 790, 90
Fegley Bruce, J., & Lodders, K. 1996, ApJL, 472, L37
Filippazzo, J., Alejandro Merchan, S., & Cruz, K. 2024, sedkit v2.0.5, Zenodo, doi:10.5281/zenodo.14169021
Filippazzo, J. C., Rice, E. L., Faherty, J., et al. 2015, ApJ, 810, 158
Gagné, J., Roy-Loubier, O., Faherty, J. K., Doyon, R., & Malo, L. 2018, ApJ, 860, 43
Gharib-Nezhad, E., Marley, M. S., Batalha, N. E., et al. 2021, ApJ, 919, 21
Golimowski, D. A., Leggett, S. K., Marley, M. S., et al. 2004, AJ, 127, 3516
Griffith, C. A., & Yelle, R. V. 1999, ApJL, 519, L85
Guest, E. R., Tennyson, J., & Yurchenko, S. N. 2024, JMoSp, 401, 111901
Hargreaves, R. J., Gordon, I. E., Rey, M., et al. 2020, ApJS, 247, 55
Hewett, P. C., Warren, S. J., Leggett, S. K., & Hodgkin, S. T. 2006, MNRAS, 367, 454
Hood, C. E., Mukherjee, S., Fortney, J. J., et al. 2024, arXiv:2402.05345
Houck, J. R., Roellig, T. L., van Cleve, J., et al. 2004, ApJS, 154, 18
Hsu, C.-C., Burgasser, A. J., Theissen, C. A., et al. 2021, ApJS, 257, 45
Justtanont, K., Feuchtgruber, H., de Jong, T., et al. 1998, A&A, 330, L17
Kirkpatrick, J. D., Cushing, M. C., Gelino, C. R., et al. 2011, ApJS, 197, 19
Kirkpatrick, J. D., Looper, D. L., Burgasser, A. J., et al. 2010, ApJS, 190, 100
Kirkpatrick, J. D., Marocco, F., Gelino, C. R., et al. 2024, ApJS, 271, 55
Kirkpatrick, J. D., Martin, E. C., Smart, R. L., et al. 2019, ApJS, 240, 19
Kirkpatrick, J. D., Reid, I. N., Liebert, J., et al. 1999, ApJ, 519, 802
Knapp, G. R., Leggett, S. K., Fan, X., et al. 2004, AJ, 127, 3553
Kumar, S. S. 1963, ApJ, 137, 1121
Lacy, B., & Burrows, A. 2023, ApJ, 950, 8
Leggett, S. K., Geballe, T. R., Fan, X., et al. 2000, ApJL, 536, L35
Leggett, S. K., Marley, M. S., Freedman, R., et al. 2007, ApJ, 667, 537
Leggett, S. K., Saumon, D., Marley, M. S., et al. 2012, ApJ, 748, 74
Li, G., Gordon, I. E., Rothman, L. S., et al. 2015, ApJS, 216, 15
Lodieu, N., Burningham, B., Day-Jones, A., et al. 2012, A&A, 548, A53
Luhman, K. L., Tremblin, P., Alves de Oliveira, C., et al. 2024, AJ, 167, 5
Marocco, F., Eisenhardt, P. R. M., Fowler, J. W., et al. 2021, ApJS, 253, 8
Martín, E. L., Basri, G., & Zapatero Osorio, M. R. 1999, AJ, 118, 1005
Martín, E. L., Lodieu, N., & del Burgo, C. 2022, MNRAS, 510, 2841
Miles, B. E., Biller, B. A., Patapis, P., et al. 2023, ApJL, 946, L6
Miles, B. E., Skemer, A. J. I., Morley, C. V., et al. 2020, AJ, 160, 63
Morley, C. V., Fortney, J. J., Marley, M. S., et al. 2012, ApJ, 756, 172
Mukherjee, S., Fortney, J. J., Batalha, N. E., et al. 2022, ApJ, 938, 107
Mukherjee, S., Fortney, J. J., Morley, C. V., et al. 2024, ApJ, 963, 73
Murakami, H., Baba, H., Barthel, P., et al. 2007, PASJ, 59, S369
Nakajima, T., Oppenheimer, B. R., Kulkarni, S. R., et al. 1995, Natur, 378, 463
Oke, J. B., Cohen, J. G., Carr, M., et al. 1995, PASP, 107, 375
Oppenheimer, B. R., Kulkarni, S. R., Matthews, K., & Nakajima, T. 1995, Sci, 270, 1478
Patten, B. M., Stauffer, J. R., Burrows, A., et al. 2006, ApJ, 651, 502
Pineda, J. S., Hallinan, G., Kirkpatrick, J. D., et al. 2016, ApJ, 826, 73
Polyansky, O. L., Kyuberis, A. A., Zobov, N. F., et al. 2018, MNRAS, 480, 2597
Rayner, J. T., Toomey, D. W., Onaka, P. M., et al. 2003, PASP, 115, 362
Rebolo, R., Osorio, M. R. Z., & Martín, E. L. 1995, Natur, 377, 129
Richard, C., Gordon, I. E., Rothman, L. S., et al. 2012, JQSRT, 113, 1276
Rigby, J., Perrin, M., McElwain, M., et al. 2023, PASP, 135, 048001
Rodrigo, C., & Solano, E. 2020, XIV.0 Scientific Meeting of the Spanish Astronomical Society (La Sociedad Española de Astronomía (SEA)), 182, https://www.sea-astronomia.es/reunion-cientifica-2020
Ryde, N., Eriksson, K., Gustafsson, B., Lindqvist, M., & Olofsson, H. 1998, Ap&SS, 255, 301
Saumon, D., & Marley, M. S. 2008, ApJ, 689, 1327
Saumon, D., Marley, M. S., Leggett, S. K., et al. 2007, ApJ, 656, 1136
Simcoe, R. A., Burgasser, A. J., Schechter, P. L., et al. 2013, PASP, 125, 270
Sousa-Silva, C., Al-Refaie, A. F., Tennyson, J., & Yurchenko, S. N. 2015, MNRAS, 446, 2337
Suárez, G., & Metchev, S. 2022, MNRAS, 513, 5701
Suárez, G., Metchev, S., Leggett, S. K., Saumon, D., & Marley, M. S. 2021, ApJ, 920, 99
Tennyson, J., & Yurchenko, S. N. 2012, MNRAS, 425, 21
Vacca, W. D., Cushing, M. C., & Rayner, J. T. 2003, PASP, 115, 389
Vrba, F. J., Henden, A. A., Luginbuhl, C. B., et al. 2004, AJ, 127, 2948
Yamamura, I., Tsuji, T., & Tanabé, T. 2010, ApJ, 722, 682
York, D. G., Adelman, J., Anderson John, E. J., et al. 2000, AJ, 120, 1579
Zalesky, J. A., Saboi, K., Line, M. R., et al. 2022, ApJ, 936, 44